Celecoxib Nanoparticles for Therapeutic Angiogenesis

Katherine Margulis,[†] Evgenios A. Neofytou,[‡] Ramin E. Beygui,[‡,§] and Richard N. Zare*,[†]

[†]Department of Chemistry, Stanford University, Stanford, California 94305-5080, United States, [‡]Department of Cardiothoracic Surgery, Falk Cardiovascular Research Center, Stanford University School of Medicine, Stanford, California 94305-5407, United States, and [§]Heart and Vascular Center, NorthBay Medical Center, 1200 B. Gale Wilson Boulevard, Fairfield, California 94533, United States

ABSTRACT
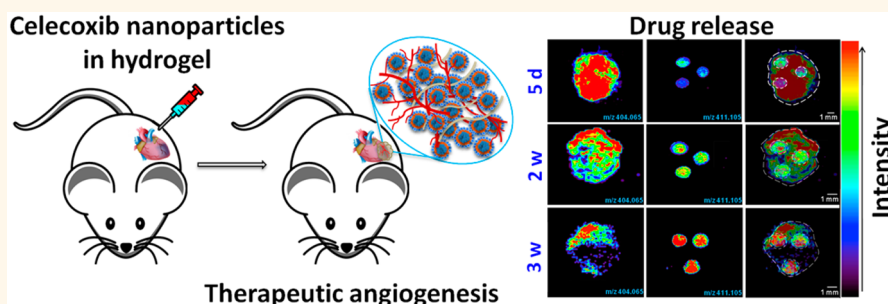
Controllable induction of blood vessel formation (angiogenesis) presents an important therapeutic goal in ischemic diseases and is also beneficial in various normal physiological processes. In this study, we have shown that nanoparticles of celecoxib, a lipophilic nonsteroidal anti-inflammatory drug, effectively evoke therapeutic angiogenesis in animal models, in both normal and ischemic organs. Celecoxib is widely considered to inhibit angiogenesis, although a recent study suggests that it can instead promote blood vessel growth in cancer cell lines. The hydrophobic nature of this drug necessitates its administration in nanoparticulate form in order to elicit a perceivable pharmacological response. We developed a facile method for nanoparticle formation by solvent extraction from microemulsions in supercritical carbon dioxide. This method exploits a spontaneous formation of nanometric domains within the microemulsion system and their rapid conversion to nanoparticles by supercritical fluid. The resultant nanoparticles were administered subcutaneously to mice in a biocompatible hydrogel, and caused a 4-fold increase in blood vessel count in normally perfused skin compared with drug-free particles. They were at least as effective in inducing angiogenesis as nanoparticles of deferoxamine, a well-established neovascularization promoter. Next, we evaluated their effect on ischemic tissues in murine model of myocardial infarction. We found that celecoxib nanoparticles were able to induce a significant vascularization of ischemic myocardium and hamper the progression of heart failure, which points toward a new approach for treating ischemia.

KEYWORDS: angiogenesis · celecoxib · nanoparticles · COX-2 inhibitors · ischemia · deferoxamine · mass spectrometry imaging

Angiogenesis, the formation of new blood vessels from an existing vasculature, plays a major role in tissue functional repair, regeneration, and growth. It is particularly crucial for preventing ischemic necrosis and for survival of any tissue damaged by hypoxia. Traditionally, therapeutic angiogenesis is induced by angiogenic growth factors (such as VEGF, FGF, EGF and PlGF), chemokines (such as MCP-1 and CXCL12/SDF-1α), or stimulation of VEGF (vascular endothelial growth factors) production using gene therapy. All these treatments require large proteins or nucleic acids to be delivered to the site of action.[1−8] These macromolecules are not only expensive, but also susceptible to fast enzymatic and chemical degradation in physiological environment, and their hydrophilicity further contributes to their extremely rapid clearance from tissues.[9−12] In addition, several reports have raised toxicity concerns regarding their use.[5,13−15] Therefore, there has been a considerable interest in evoking angiogenesis by alternative therapeutic systems,[16] especially by localized delivery of nanoparticles of small-molecule drugs that show some pro-angiogenic properties.[17−19] Finding a suitable drug is challenging, as many of candidate compounds are hydrophilic or suffer from appreciable toxicity. In our experimental search for an

efficient pro-angiogenic treatment, we found that nanoparticles of celecoxib, a small lipophilic painkiller, the specific inhibitor of the cyclooxygenase-2 (COX-2) enzyme, can successfully induce a substantial local vascularization *in vivo* in both normal and ischemic tissues. Celecoxib, (4-[5-(4-methylphenyl)-3-(trifluoromethyl)-1*H*-pyrazol-1-yl]benzenesulfonamide), displays a low aqueous solubility (3−7 μg/mL),[20] which results in its insufficient bioavailability after oral administration and hinders the development of parenteral dosage forms.[20] This necessitates its administration in nanoparticulate form.[21] Hence, amphiphile-polymer nanoparticles of celecoxib were developed in this study.

Currently, there is a contradictory evidence in the literature regarding the effect of celecoxib on vascularization. While it is widely accepted that this drug down-regulates angiogenesis through various pathways,[22−26] few recent reports suggest that in tumors celecoxib might instead promote vascularization.[27,28] One study found that circulating VEGF levels were increased in breast cancer patients treated with celecoxib.[27] Another study reported on the induction of angiogenesis by celecoxib in several different cancer cell lines and tumor xenografts, and a possible mechanistic pathway for this effect was proposed.[28] Yet another study demonstrated elevation of several pro-angiogenic proteins after systemic administration of celecoxib to familial adenomatous polyposis patients.[29] To the best of our knowledge, celecoxib has never been proposed for therapeutic angiogenesis or tested for this purpose in normally perfused or ischemic organs.

In our study, nanoparticles of celecoxib were formed by supercritical carbon dioxide (CO_2) extraction from a volatile oil-in-water microemulsion in Solution-Enhanced Dispersion by Supercritical fluids (SEDS) setup.[30,31] This method exploits a spontaneous formation of nanometric domains within the microemulsion system, which serve as templates for nanoparticle synthesis.[32] Extracting solvents with supercritical CO_2 causes particle nucleation and growth within the nanometric domains of the microemulsion, whereas the particles are formed at one step and with minimal heating. To localize the nanoparticles at the desired site of action, they were embedded in an injectable hydrogel.

This hydrogel was injected subcutaneously to healthy mice so as to evaluate the angiogenic potential in normally perfused skin and to compare the efficacy of this treatment to nanoparticles of deferoxamine, a well-established vascularization promoter.[17−19] A method based on Desorption Electrospray Ionization Mass Spectrometry Imaging (DESI-MSI) was developed for tracking the release of the drug *in vivo*. Next, the efficacy of this treatment in ischemia was evaluated in murine heart attack models. The mice with permanent occlusion of coronary artery were treated with celecoxib nanoparticles in the hydrogel injected around the infarct area. Blood vessel formation in the heart, heart muscle enlargement, and functional damage were monitored for one month.

RESULTS AND DISCUSSION

Formation of Nanoparticles. Celecoxib nanoparticles were prepared by supercritical CO_2 extraction from a volatile oil-in-water microemulsion, which is schematically presented in Figure 1A. As the dispersed phase, the microemulsion contained *n*-butyl acetate (nBuAc) in which celecoxib (CXB) and poly lactide-*co*-glycolide (75:25) (PLGA) were dissolved. Optical transparence and low viscosity of this system demonstrated nanometric dimensions of the dispersed domains. The mean droplet size, as measured by dynamic light scattering (DLS), was 12 ± 1 nm. The conductivity was 1.9 mS/cm, which was about 3 orders of magnitude greater than the conductivity of the organic phase, which is expected for an oil-in-water inner structure. The microemulsion was stabilized by soybean phosphatidylcholine (SbPC), glycyrrhizinic acid salts (ammonium glycyrrhizinate (AG) and dipotassium glycyrrhizinate (DG)), and *tert*-butanol (tBuOH). The specific composition was selected experimentally based on size, drug content, and dispersibility of the particles generated from the system. The composition of the selected microemulsion is given in Table 1. Solvent extraction from this microemulsion by supercritical CO_2 yielded a solid powder composed of spherical nanoparticles (Figure 1C). The powder theoretical composition is given in Table 1; all its inactive components are listed by the FDA as Generally Regarded As Safe (GRAS). Celecoxib was present in this powder in the amorphous form (Supporting Information (SI), Figure S1B) and its content was found to be 17.5 ± 1.4 wt %. The powder was freely dispersible in water to yield a stable suspension of particles with an average size of 110 ± 3 nm (by DLS) (Figure 1B), and a negative surface charge, with the mean ζ-potential of −31 ± 1 mV (pH = 6). The size of the particles in the powder was also confirmed by Scanning Electron Microscopy (SEM) (Figure 1C). The increase in the size of the particles compared with the initial microemulsion droplet size can be attributed to the aggregation of the droplets during solvent removal.[33] Measured ζ-potential was high enough in its absolute value to provide electrostatic stabilization to the resultant particles, stemming from the absorption of negatively charged surfactants[34−36] and from the possible presence of the anionic polymer on the surface. There was no significant change in the mean size or the mean ζ-potential of the particles in water after 5 h.

At the next stage, the nanoparticles were dispersed (5.5% w/v) in an injectable hydrogel for immobilization at the site of injection.[37] The hydrogel was composed of biocompatible and biodegradable polymers, poly-(vinyl alcohol) (MW 89 000−98 000 Da, PVA, 10 wt %)
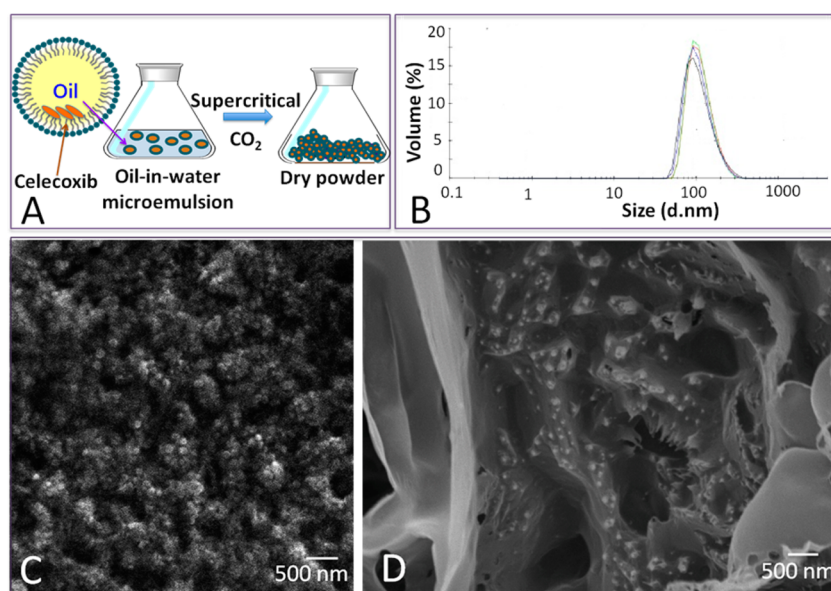
Figure 1. Celecoxib nanoparticles formation and characterization. (A) Schematic representation of nanoparticle formation process; (B) particle size measurements in water by DLS; (C) SEM image of nanoparticles in powder; (D) SEM image of nanoparticles embedded in hydrogel (dried).

TABLE 1. Compositions of Celecoxib Containing Microemulsion (CXB ME), Nanoparticulate Powder Obtained after SEDS Process (CBX NP), and Nanoparticle-Loaded Hydrogel (CXB NP HGL)

% wt	CXB	PLGA	SbPC	AG	DG	H₂O	nBuAc	tBuOH	PVA	PVP
CXB ME	3.7	0.2	5.3	8.8	2.1	40.4	18.3	21.2		
CXB NP	18.4	1	26.4	43.8	10.4					
CXB NP HGL	1.0	0.1	1.4	2.4	0.6	82.2			9.5	2.8

and polyvinylpyrrolidone (average MW 40 000 Da, PVP, 3 wt %),[38] physically cross-linked together at low temperature by a freeze−thawing cycle. The hydrogel was easily injectable exhibiting shear-thinning behavior, and it did not contain any toxic monomers or cross-linkers. The nanoparticles were readily dispersible in the gel and their homogeneous distribution was confirmed by SEM (Figure 1D).

***In Vivo* Vascularization.** A volume of 100 μL of the resultant particle-loaded hydrogel containing 0.96 ± 0.08 mg of celecoxib was injected subcutaneously into dorsal sites of mice to monitor the angiogenesis in the normally perfused skin tissue. The hydrogel restricted spatial distribution of the particles. As it can be seen in Figure 2A(I−II),B(II),C(II) after only 5 days following the injection, a profound vascularization occurred around the hydrogel location. Noticeable capillary enlargement as well as *de novo* capillary sprouting could be seen in the region around the drug-loaded hydrogel. The neovascularization effect could also be detected by staining for CD31 antibody and comparing treated *vs* untreated skin (treated with drug-free vehicle control).

CD31 staining demonstrated a dense network of microscopic blood vessels formed in the drug-treated tissue within 5 days post injection (Figure 2B(II),C(II)) with a 4-fold increase in blood vessel count compared to the drug-free vehicle control group (two-tailed unpaired Student's *t* test, $p = 0.001$) (Figure 2B(I),C(I)). The treated mice were closely monitored up to one-month postinjection, and no signs of distress were observed. Vascularization around the hydrogel area and the intact hydrogel observed 3 weeks following the injection are shown in Figures 2A(III−V). After 4 weeks, in 50% of the tested mice, the gels had visually disappeared, evidencing a biodegradable nature of this scaffold. However, the extensive capillary network at the site of treatment stayed intact, demonstrating its therapeutic feasibility (Figure S2B(II)). It is noteworthy that the increased vascularization was restricted to the treated region and could be attributed to the high local concentration of the drug. Nevertheless, the systemic effects associated with this treatment are expected to be less pronounced compared with the effects of therapeutically relevant oral dosages in humans. Thus, celecoxib dosage of 400 mg/day is recommended for persistent pain. This dosage corresponds to a murine dosage of about 0.14 mg/day (by body weight) or to 1.76 mg/day (by body surface area). The hydrogel in our study releases its drug content gradually (see Drug Release Studies section below), at an average rate of 0.036 mg/day. Although a systemic absorption of celecoxib from the orally administered capsule is only about 30%,[20] the drug released from the hydrogel will reach lower systemic concentration, even if 100% bioavailability is assumed.

Efficacy *versus* Nanoparticles of Established Vascularization Promoter. The angiogenic potential of celecoxib in nanoparticles was compared with that of deferoxamine,
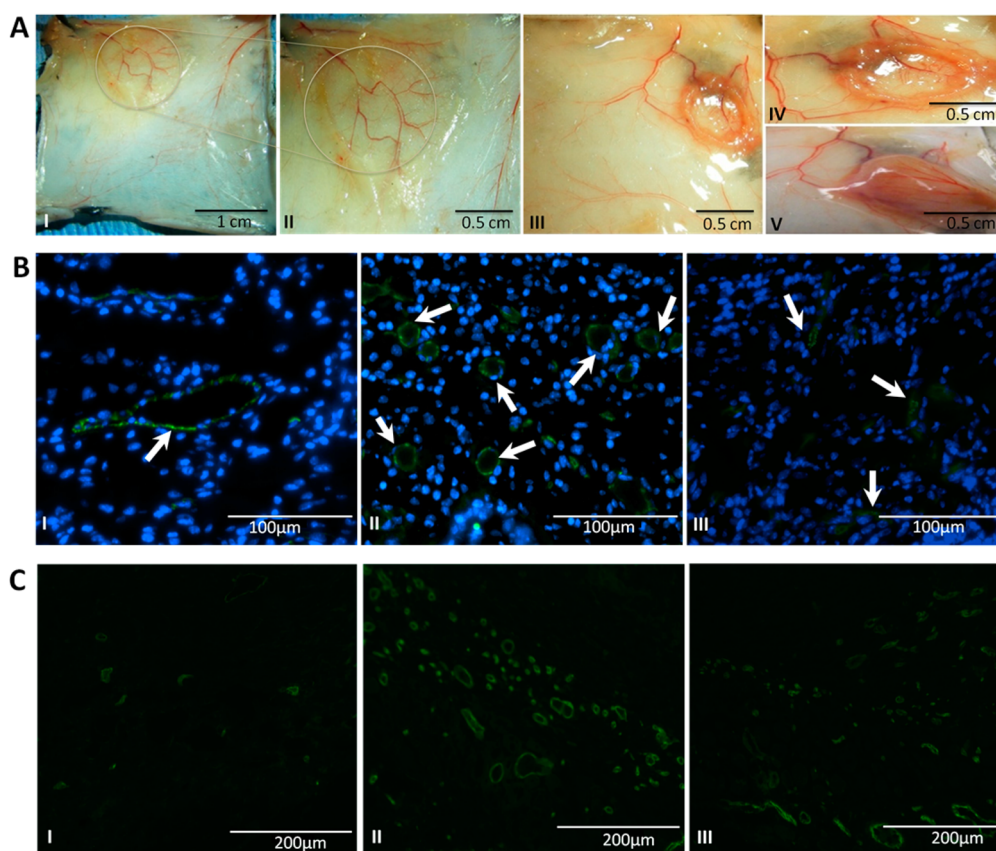
Figure 2. Vascularization in normally perfused murine skin tissue. (A) Images of the area underneath and around celecoxib nanoparticles containing hydrogel: (I, II) 5 days postinjection; (III—V) 3 weeks postinjection. (B and C) CD31 staining of microscopic blood vessels around the hydrogel region 5 days postinjection. Green color indicates blood vessels, blue is cell nuclei. Some blood vessels are marked by arrows. (I) Drug-free vehicle control hydrogel; (II) celecoxib nanoparticles containing hydrogel; (III) deferoxamine nanoparticles containing hydrogel.

a drug that is extensively studied as a treatment for induction of therapeutic angiogenesis. Deferoxamine was proven to effectively promote blood vessel formation.[17−19] However, the potential utilization of this drug is hindered by its high water solubility, appreciable toxicity at large doses, and very rapid *in vivo* clearance.[39,40] We encapsulated this drug in nanoparticles prepared by supercritical CO_2 extraction from a reverse, water-in-oil microemulsion. The microemulsion preparation is described in the SI. The particles generated from this microemulsion were freely dispersible in water and had a mean size of 72 ± 6 nm (by DLS), a mean ζ-potential of -41 ± 1 mV (pH = 6), and an average drug loading of 3.4 ± 0.1 wt %. These particles provided extended release of the drug for over 21 days with the initial burst effect typical to hydrophilic drugs[41] (Figure S2A). The chemical compositions of the microemulsion and the particles are given in Table S1. These particles were incorporated (30% w/v) into the hydrogel described above, and injected subcutaneously to dorsal sites of mice. A significantly greater particle concentration was required to achieve the therapeutic effect with deferoxamine nanoparticles as compared to celecoxib, due to a limited attainable drug loading stemming from the

high aqueous solubility of deferoxamine. A noticible neovascularization effect was observed after 5 days; however, it was morphologically inferior to celecoxib-induced vascularization (Figure S2B(I)). While well-developed and visually prominent blood vessels prevailed in the celecoxib case, in the case of deferoxamine, smaller and less distinct blood vessels were observed. CD31 immunohistochemical staining, which reveals microscopic blood vessels, demonstrated a slight superiority of celecoxib over deferoxamine (in average 20% greater blood vessel count), for microscopic vessels. Compared with the drug-free vehicle control group, deferoxamine demonstrated a 3.2-fold increase (two-tailed unpaired Student's t test, $p = 0.01$) in microscopic blood vessel count (Figure 2B(III),C(III)). It is noteworthy that deferoxamine, similarly to the majority of small-molecule drug with proangiogenic properties, promotes angiogenesis by preventing a degradation of hypoxia inducible factor-1 α-subunit (HIF-1α), virtually simulating hypoxic conditions. Outcomes of several recent studies suggest that celecoxib activates physiological pathway independent of HIF-1α stabilization.[28,29] Thus, Dovizio *et al.*[29] proposed that large oral doses of celecoxib in humans (800 mg/day) inhibit vascular COX-2 dependent prostacyclin (PGI_2),
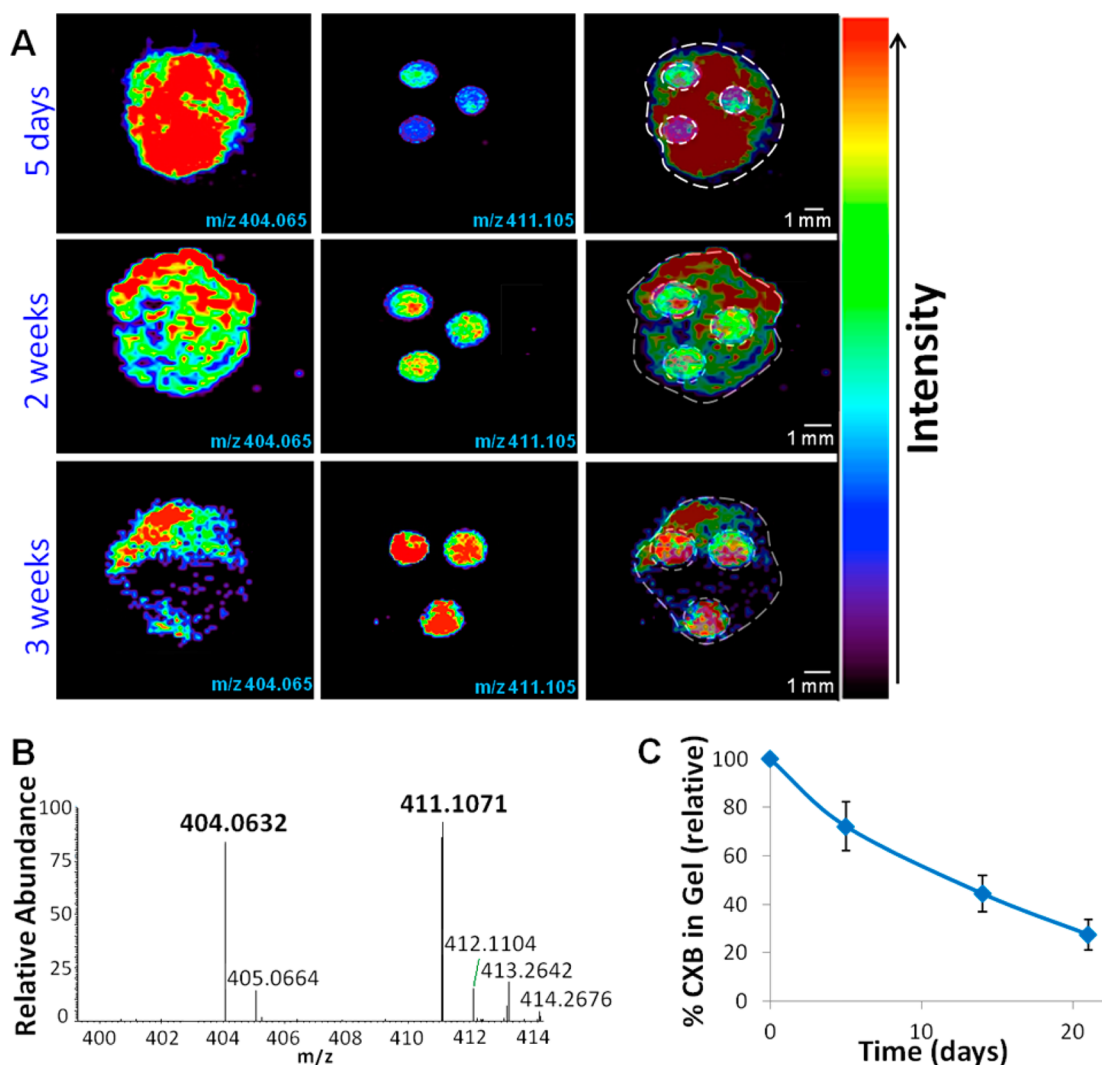
Figure 3. Release of celecoxib from the hydrogel *in vivo*. (A) Spatial distributions of celecoxib as detected by DESI-MSI: the left column displays the distribution of the drug in sections of the gels extracted from mice after 5, 14, and 21 days following the injection; the middle column shows the image of the isotopic drug distribution after spiking on the hydrogel sections. The concentration of the spiked solution is constant in all samples and the increase in signal intensity with decreasing celecoxib concentration originates from signal suppression. The right column demonstrates superimposition of the images. (B) DESI mass spectrum of the spotted region. (C) The fraction of the mean celecoxib concentration remaining in the hydrogel *in vivo* plotted against the time following the injection (the error bars represent standard deviation).

which leads to the release of angiogenic mediators from platelets and their increased expression in endothelial cells. Xu *et al.*[28] explored celecoxib-mediated angiogenesis in multiple glioma cell lines and found that it is independent of hypoxic pathway and requires both mitogen-activated protein kinase p38-MAPK and Sp1 transcription factor. Consequently, celecoxib and hypoxia demonstrated an additive effect on elevation of VEGF in glioma cancer cells *in vitro*.[28]

It is thus expected that nanoparticles of celecoxib would present a promising therapeutic candidate for induction of angiogenesis in ischemic tissues, where HIF-1α is already elevated.

Drug Release Studies. Drug release studies from the hydrogels containing celecoxib nanoparticles *in vivo* were performed by DESI-MSI[42−45] in positive ion mode, and are presented in Figure 3. The concentration and

the spatial distribution of the drug remaining in the hydrogels harvested from mice at various time intervals following the subcutaneous injection were detected by mapping the chemical composition of the hydrogel in a two-dimensional manner.[43−45] To desorb and ionize celecoxib molecules, a beam of charged solvent droplets was directed to the sample, extracting the drug into secondary droplets, which were subsequently analyzed by the mass spectrometer. A two-dimensional distribution image with relative signal intensity was generated for *m/z* 404.06, representative of sodium adduct of celecoxib. For signal intensity standardization, each gel was spiked trice with deuterated isotope of celecoxib (D7-CXB, *m/z* 411.10) at a known concentration (3×10^{-3} M), and the normalized signal intensity (CXB/D7-CXB) was found to be directly proportional to celecoxib concentration (Figure S1A).
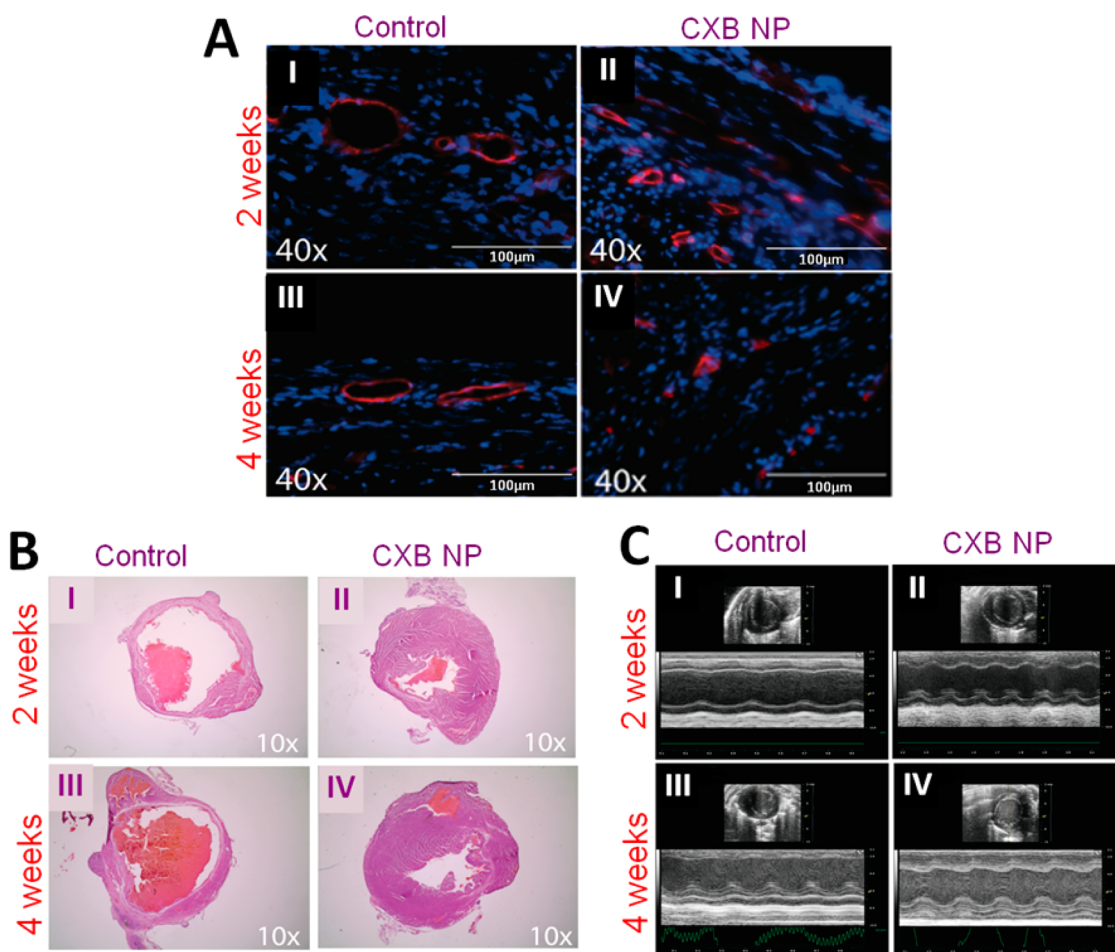
Figure 4. Treatment efficacy in mice with permanent LAD ligation 2 and 4 weeks postinjection. (A) CD31 staining of blood vessels at the infarction area. Red color indicates blood vessels, blue is cell nuclei. (B) Myocardium morphology, H&E stained. (C) M-mode echocardiography.

On the basis of concomitant detection of the drug and its deuterated isotope from the surface of longitudinal section of the gel, the release of the drug could be rapidly monitored. Such normalization allowed to control variability in relative ion intensity between different measurements and to overcome mutual signal suppression between the two molecules due to competing processes in the ionization mechanism.[46]

It was also confirmed that the drug encapsulated in nanoparticles could be readily identified by this technique. As it can be seen in Figure 3, the drug was gradually released from the gel *in vivo*, reaching about 30% from its initial concentration in 3 weeks. As it was already mentioned above, the gel lost its integrity with time, which could partially account for the drug release.

Drug Crystallinity. As can be seen in Figure S1B, celecoxib is amorphous in the nanoparticles and it preserves its amorphous character in the hydrogel *in vivo*, for the duration of the experiment, *i.e.*, at least for 3 weeks. X-ray diffractograms were obtained for the gels that were harvested from mice after 5 and 21 days

and subsequently lyophilized. The diffractograms were compared to the diffractogram of crystalline celecoxib and to the diffractogram of the physical mixture of all powder components incorporated 3.5% (w/v) to the hydrogel prior to drying, roughly indicative of the concentration of celecoxib in the hydrogel 5 days following the injection. Peaks of crystalline celecoxib could be clearly observed in both reference diffractograms, but not in the diffractograms of the hydrogels harvested from mice. It was also verified that crystalline celecoxib can be detected in the hydrogel at concentrations as low as 0.14 wt %, about 14% of the initial concentration of the drug in the gel. Crystallization inhibition effect in the hydrogels can be attributed to both AG,[47] which is a part of the amphiphile layer of the particles, and to PVP[48] and PVA,[49] which are the integral components of the hydrogel.

Efficacy in Myocardial Infarction Models. To evaluate therapeutic potential of celecoxib nanoparticles in ischemic tissue, a treatment efficacy study was performed in mice with the permanent ligation of the left anterior descending artery (LAD). This procedure leads
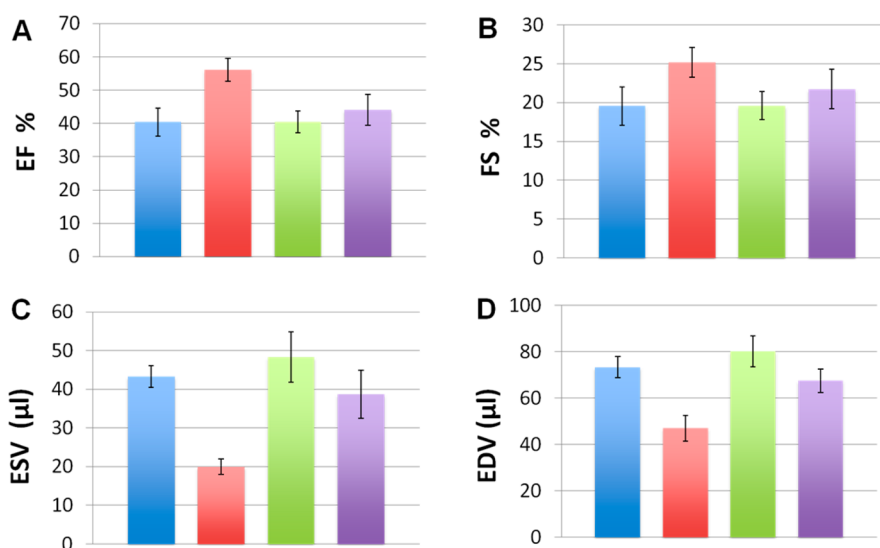
Figure 5. Cardiac function parameters assessed by echocardiography: (A) ejection fraction; (B) fractional shortening; (C) end systolic volume; (D) end diastolic volume. All graphs show mean value $\pm$ standard error. Blue columns represent control group and red ones represent treated group at two week time point (two-tailed unpaired Student's *t* test, $p < 0.05$); green columns stand for control group and purple ones for treated group at one month ($p \geq 0.05$).

to a continuous heart attack, while the onset of heart muscle ischemia is almost immediate. Twenty mice were employed for this study; all developed well-defined infarction regions following the procedure. Ten mice were treated with celecoxib nanoparticles in the hydrogel (100 μL of the hydrogel containing 0.96 $\pm$ 0.08 mg of the drug) injected around the area of infarcted myocardium and the rest were administered drug-free vehicle control in the hydrogel. The animals were observed for one month. The vital signs, heart function, myocardium structural changes, heart volume, and infarct perfusion were monitored at two and four-week time points following the ligation.

Overall 6 out of 10 mice (60%) survived in the control group, while 100% survival rate was seen in the treated group. A prominent neovascularization of the infarcted region was observed in the treated group (Figure 4A) at both monitoring time points. Myocardial muscle morphology showed a markedly less pronounced left ventricular (LV) wall thinning and lumen dilatation in the treated group at both time points (Figure 4B). These parameters are closely associated with heart failure, possible scarring and poor heart muscle contractility.[50,51]

Echocardiography showed less distinct changes in LV function and a smaller expansion of chamber dimensions in the treated group at 2 weeks following the ligation (Figures 4C and 5). This was attested by lower end diastolic and end systolic volumes (EDV and ESV, respectively), and larger ejection fraction (EF) and fractional shortening (FS) ($p < 0.05$) (Figure 5). However, at 4 weeks, the differences in these parameters between two groups were less prominent, and the statistical significance could not be established ($p \geq 0.05$) (Figure 5).

No thrombotic events associated with the inhibition of vascular production of PGI_2 and none of thromboxane A_2 by celecoxib[52] were recorded in this study. It is noteworthy that the investigated treatment is short-term and is not expected to result in high systemic levels of the drug for prolonged periods of time, which predisposes to thrombotic effects. However, a larger study is required to establish its cardiovascular safety.

It is evident that the treatment can attenuate cardiac remodeling and hamper the transition to heart failure. Yet, it is well accepted that a delivery of a single proangiogenic factor is usually insufficient to promote long-term cardiac repair following myocardial infarction.[53] Optimization of proangiogenic therapy might combine stimulation of angiogenesis with vessel maturation and the use of stem/progenitor/endothelial cell therapies[53,54] so as to attain a permanent heart regeneration.

CONCLUSIONS

Nanoparticles of the specific COX-2 inhibitor, celecoxib, formed by solvent extraction from a volatile oil-in-water microemulsion in supercritical CO_2, are capable of inducing angiogenesis in normally perfused and ischemic organs. In fact, a 4-fold increase in blood vessel count was achieved in skin tissue treated with celecoxib nanoparticles, indicating a significant angiogenic response. This response is comparable to the vascularization reported following a successful VEGF165 gene therapy (3-fold increase in total blood vessel count and 4.4-fould increase in number of small capillaries in ischemic dog hearts).[55] Furthermore, the efficacy of celecoxib nanoparticles in angiogenesis induction was at least as prominent as the efficacy of nanoparticles

of deferoxamine, a well-establish neovascularization promoter, extensively studied as therapeutic angiogenesis inducer. Nanoparticles of celecoxib are expected to exhibit several advantages over other delivery systems of small-molecule drugs used for therapeutic angiogenesis, including deferoxamine. Celecoxib is likely to have a longer residence time in tissues owing to its lipophilicity, its systemic toxicity is low, and a variety of possible administration routes are available for this drug including transdermal.[56] Additionally, celecoxib was proven to elevate VEGF by a pathway alternative to hypoxia and therefore it may be advantageous for vascularization of ischemic tissues when used alone or in combination with HIF-1α stabilizers.

Prominent vascularization of infarcted myocardium was demonstrated in mice with heart attack treated with celecoxib nanoparticles. Myocardial muscle morphology showed a markedly less pronounced LV wall thinning and lumen dilatation in the treated group 2 and 4 weeks after the onset of the heart attack. Preservation of LV function and a smaller expansion of heart dimensions were clearly seen in the treated group 2 weeks after the onset of the heart attack, but after 4 weeks, the difference between the treatment and the control groups was less prominent. Thus, celecoxib nanoparticles may impede the progression of coronary hypertrophy and functional cardiac damage caused by permanent LAD ligation, and hamper the transition to heart failure. We envision that such a system will be used in combination with cell therapy to achieve a long-term cardiac repair, and may be translated into clinic by exploiting several potential delivery routes. These routes include catheter-based endocardial injection of the hydrogel to ischemic areas and systemic delivery of the particles modified with hypoxia-targeting peptides on their surface. Such modification may allow the particles to accumulate preferentially at the site of cardiac damage.[57]

Novel pro-angiogenic treatment modalities are urgently required in a wide variety of pathological conditions.[13] While our initial feasibility study was conducted in myocardial infarction model, its outcome may have impact on treating other ischemic disorders, such as peripheral ischemia in diabetes, ischemic stroke, traumatic injuries and more.

METHODS

Formation of Celecoxib-Loaded Microemulsion. The exact concentrations of the components used for the microemulsion formation are summarized in Table 1. The components were mixed together and the mixture was allowed to equilibrate at 45 °C until a transparent isotropic system was formed. Droplet size distributions in the microemulsion, as well as its conductivity, were measured by Nano-ZS90 Zetasizer (Malvern, U.K.). Each sample was prepared in triplicate and triplicate repetitions of each measurement were taken.

Converting Celecoxib-Loaded Microemulsion to Nanoparticles. The solvents were extracted from the microemulsion by the SEDS setup based on a modified commercial instrument (SAS-50, Thar Technologies, PA, see SI for details).

The dispersibility and the size of the particles were characterized by dispersing the dry powder 0.1−10 wt % in deionized water and vortexing for 30 s to ensure homogeneous dispersion. The size distribution and ζ-potential measurements of the particles were performed in 0.1 wt % dispersion at room temperature using a Nano-ZS90 Zetasizer (Malvern, U.K.). Celecoxib content in the powder was determined by Electrospray Ionization Mass Spectrometry using D7-CXB as an internal standard (SI). Each sample was prepared in triplicate and triplicate repetitions of each measurement were taken.

Hydrogel Formation. The hydrogel was formed by first dissolving PVA (10 wt %) and PVP (3 wt %) in hot water (~90 °C) to obtain a moderately viscous solution. Celecoxib nanoparticulate powder was homogeneously dispersed 5.5% (w/v) in the solution upon cooling by vortexing for 3 min. No visible particulates were observed in the resultant suspension. A volume of 100 μL of the suspension was loaded into 1 mL polycarbonate syringe (BD Luer-Lok disposable syringe) and stored at −20 °C for 12 h to allow physical cross-linking of the polymers. After a thawing period of 2 h at room temperature, elastic, shear-thinning hydrogels were obtained, and could be easily injected when subjected to the pressure in the syringe.

***In Vivo* Skin Vascularization and Histology.** The hydrogels were sterilized under UV irradiation for 2 h and injected subcutaneously into dorsal sites of adult male C57BL/6 mice (10 weeks old). The animals were treated according to the animal care and use program at Stanford University, which meets the requirements of the Federal Law (89-544 and 91-579) and NIH regulations, and is also accredited by the American Association for Accreditation of Laboratory Animals (AAALAC). The animals were randomly divided into three groups (20 subjects each): (1) injected with hydrogel loaded with celecoxib nanoparticles; (2) injected with drug-free vehicle (hydrogel containing drug-free nanoparticles); (3) injected with hydrogel loaded with deferoxamine nanoparticles. (See SI for the detailed description of deferoxamine nanoparticle formation). Local vascularization was monitored after 5, 14, 21, and 30 days following the injection. The mice were euthanized, subcutaneous dorsum was dissected, and the remaining gels with the adjacent skin were harvested. Vascularization of the area around and under the hydrogel was evaluated morphologically against the untreated skin and against the skin treated with the drug-free vehicle by two blind observers. The detection of the microscopic blood vessels was performed by CD31 immunohistochemical staining (SI). Green color indicates blood vessels (CD31), while blue one indicates cell nuclei (stained with DAPI (4',6-diamidino-2-phenylindole)). Three samples were observed for each mouse and the average of 11 high-power fields were acquired per sample. The images were digitally montaged using Adobe Photoshop CS6, counted by pixel intensity, and normalized by the acquired area. Statistical analysis was performed using a two-tailed unpaired Student's t test. Values of $p < 0.05$ were considered statistically significant.

Drug Release by DESI-MSI. To assess the concentration of celecoxib remaining in the hydrogels *in vivo* as the function of time, at a first step a calibration curve was acquired using the premade hydrogel spheres with known varying concentrations of celecoxib particles (SI).

The hydrogels harvested from mice at various time intervals postinjection (after 5, 14, and 21 days) were dissected to 25 μm-thick sections and carefully spotted three times with 0.17 μL solution of the internal standard: 3×10^{-3} M of D7-CXB dissolved in 50% methanol, so as to obtain round spots of ~1.5 mm in diameter. The spotted sections were imaged by DESI-MSI in positive ion mode by tracking ion spatial distribution for sodium adducts of the drugs (at m/z 404.06 for celecoxib and at m/z 411.10 for its deuterated counterpart). A lab-built

DESI-MS imaging ion source[42,44,45] coupled to an LTQ-Orbitrap XL Mass Spectrometer (Thermo Fisher Scientific, MA) was used for imaging, and the mass spectra were acquired using Orbitrap as the mass analyzer at 60 000 resolving power in the range m/z 300−500. The normalized signal intensity was calculated for each spot (defined as a region of interest, ROI) and the mean normalized signal intensities were then derived for each gel. On the basis of the calibration curve, they were indicative of the mean celecoxib concentration in the gel.

Efficacy in Myocardial Infarction Models. The LAD ligations were performed according to the published protocol[58] in 20 12 weeks old male C57BL/6 mice. Each ligation was performed with one single stitch, forming almost immediate ischemia. Ten mice received drug-loaded nanoparticles in the hydrogel around the ischemic region following the ligation, while the other 10 received the control (drug-free nanoparticles in the hydrogel). The mice were closely monitored for one month. After 2 weeks they underwent echocardiography, which was performed using the General Electric Vivid 7 Dimension imaging system equipped with a 13-MHz linear probe (General Electric, Milwaukee, WI). Animals received continuous inhaled anesthetic (1.5−2% isofurane), for the duration of the imaging session, and were imaged in the supine position. Echocardiography was performed by an independent operator. M-mode short-axis views of the left ventricle were recorded. Analysis of the M-mode images was performed using GE built-in analysis software.[59] Statistical analysis was performed using a two-tailed unpaired Student's t test. Values of $p < 0.05$ were considered statistically significant.

Then, 3 subjects in each treatment group were euthanized for testing heart morphology, histology and vascularization. After performing paraffin sections, slides were stained with H&E (hematoxylin and eosin) or trichrome to visualize fibrotic tissue. CD31 immunohistochemical staining was employed to visualize microscopic blood in the infarct region (see above and SI). Red color indicates blood vessels (CD31), while blue represents cell nuclei. All the experiments were repeated after one month.

Conflict of Interest: The authors declare no competing financial interest.

REFERENCES AND NOTES

1. Gupta, R.; Tongers, J.; Losordo, D. W. Human Studies of Angiogenic Gene Therapy. *Circ. Res.* **2009**, *105*, 724–736.

2. Chu, H.; Wang, Y. Therapeutic Angiogenesis: Controlled Delivery of Angiogenic Factors. *Ther. Delivery* **2012**, *3*, 693–714.

3. Ferrara, N.; Kerbel, R. S. Angiogenesis as a Therapeutic Target. *Nature* **2005**, *438*, 967–974.

4. Deveza, L.; Choi, J.; Yang, F. Therapeutic Angiogenesis for Treating Cardiovascular Diseases. *Theranostics* **2012**, *2*, 801–814.

5. Markkanen, J. E.; Rissanen, T. T.; Kivela, A.; Yla-Herttuala, S. Growth Factor-linduced Therapeutic Angiogenesis and Arteriogenesis in the Heart-Gene Therapy. *Cardiovasc. Res.* **2005**, *65*, 656–664.

6. Al Sabti, H. Therapeutic Angiogenesis in Cardiovascular Disease. *J. Cardiothorac. Surg.* **2007**, *2*, 49–56.

7. Kumar, V. A.; Taylor, N. L.; Shi, S. Y.; Wang, B. K.; Jalan, A. A.; Kang, M. K.; Wickremasinghe, N. C.; Hartgerink, J. D. Highly Angiogenic Peptide Nanofibers. *ACS Nano* **2015**, *9*, 860–868.

8. Ho, T. K.; Shiwen, X.; Abraham, D.; Tsui, J.; Baker, D. Stromal-Cell-Derived Factor-1 (SDF-1)/CXCL12 as Potential Target of Therapeutic Angiogenesis in Critical Leg Ischaemia. *Cardiol. Res. Pract.* **2012**, *2012*, 143209.

9. Gu, F.; Amsden, B.; Neufeld, R. Sustained Delivery of Vascular Endothelial Growth Factor with Alginate Beads. *J. Controlled Release* **2004**, *96*, 463–472.

10. Kim, S. H.; Jeong, J. H.; Lee, S. H.; Kim, S. W.; Park, T. G. PEG Conjugated VEGF siRNA for Anti-Angiogenic Gene Therapy. *J. Controlled Release* **2006**, *116*, 123–129.

11. Roskoski, R., Jr. Vascular Endothelial Growth Factor (VEGF) Signaling in Tumor Progression. *Crit. Rev. Oncol. Hematol.* **2007**, *62*, 179–213.

12. Lauer, G.; Sollberg, S.; Cole, M.; Flamme, I.; Sturzebecher, J.; Mann, K.; Krieg, T.; Eming, S. A. Expression and Proteolysis of Vascular Endothelial Growth Factor is Increased in Chronic Wounds. *J. Invest. Dermatol.* **2000**, *115*, 12–8.

13. Bhatia, S. Translation of Pro-Angiogenic and Anti-Angiogenic Therapies into Clinical Use. In *Mechanical and Chemical Signaling in Angiogenesis*; Reinhart-King, C. A., Ed.; Springer: Berlin-Heidelberg, 2013; pp 261−278.

14. Vajanto, I.; Rissanen, T. T.; Rutanen, J.; Hiltunen, M. O.; Tuomisto, T. T.; Arve, K.; Narvanen, O.; Manninen, H.; Rasanen, H.; Hippelainen, M.; et al. Evaluation of Angiogenesis and Side Effects in Ischemic Rabbit Hindlimbs after Intramuscular Injection of Adenoviral Vectors Encoding VEGF and LacZ. *J. Gene Med.* **2002**, *4*, 371–380.

15. Le Cras, T. D.; Spitzmiller, R. E.; Albertine, K. H.; Greenberg, J. M.; Whitsett, J. A.; Akeson, A. L. VEGF Causes Pulmonary Hemorrhage, Hemosiderosis, and Air Space Enlargement in Neonatal Mice. *Am. J. Physiol. Lung Cell. Mol. Physiol.* **2004**, *287*, L134–L142.

16. Bartczak, D.; Muskens, O. L.; Sanchez-Elsner, T.; Kanaras, A. G.; Millar, T. M. Manipulation of in Vitro Angiogenesis Using Peptide-Coated Gold Nanoparticles. *ACS Nano* **2013**, *7*, 5628–5636.

17. Jiang, X.; Malkovskiy, A. V.; Tian, W.; Sung, Y. K.; Sun, W.; Hsu, J. L.; Manickam, S.; Wagh, D.; Joubert, L. M.; Semenza, G. L.; et al. Promotion of Airway Anastomotic Microvascular Regeneration and Alleviation of Airway Ischemia by Deferoxamine Nanoparticles. *Biomaterials* **2014**, *35*, 803–813.

18. Duscher, D.; Neofytou, E.; Wong, V. W.; Maan, Z. N.; Rennert, R. C.; Inayathullah, M. Transdermal Deferoxamine Prevents Pressure-Induced Diabetic Ulcers. *Proc. Natl. Acad. Sci. U. S. A.* **2015**, *112*, 94–99.

19. Ko, S. H.; Nauta, A.; Morrison, S. D.; Zhou, H.; Zimmermann, A.; Gurtner, G. C.; Ding, S.; Longaker, M. T. Antimycotic Ciclopirox Olamine in the Diabetic Environment Promotes Angiogenesis and Enhances Wound Healing. *PLoS One* **2011**, *6*, e27844.

20. Paulson, S. K.; Vaughn, M. B.; Jessen, S. M.; Lawal, Y.; Gresk, C. J.; Yan, B.; Maziasz, T. J.; Cook, C. S.; Karim, A. Pharmacokinetics of Celecoxib after Oral Administration in Dogs and Humans: Effect of Food and Site of Absorption. *J. Pharmacol. Exp. Ther.* **2001**, *297*, 638–645.

21. Keck, C. M.; Muller, R. H. Drug Nanocrystals of Poorly Soluble Drugs Produced by High Pressure Homogenisation. *Eur. J. Pharm. Biopharm.* **2006**, *62*, 3–16.

22. Kumar, B. N.; Rajput, S.; Dey, K. K.; Parekh, S.; Mazumdar, A.; Mandal, M. Celecoxib Alleviates Tamoxifen-Instigated Angiogenic Effects by ROS-Dependent VEGF/VEGFR2 Autocrine Signaling. *BMC Cancer* **2013**, *13*, 273–288.

23. Klenke, F. M.; Gebhard, M. M.; Ewerbeck, V.; Abdollahi, A.; Huber, P. E.; Sckell, A. The Selective Cox-2 Inhibitor Celecoxib Suppresses Angiogenesis and Growth of Secondary Bone Tumors: an Intravital Microscopy Study in Mice. *BMC Cancer* **2006**, *6*, 9–17.

24. Wang, L.; Chen, W.; Xie, X.; He, Y.; Bai, X. Celecoxib Inhibits Tumor Growth and Angiogenesis in an Orthotopic Implantation Tumor Model of Human Colon Cancer. *Exp. Oncol.* **2008**, *30*, 42–51.

25. Ballabh, P.; Xu, H.; Hu, F.; Braun, A.; Smith, K.; Rivera, A.; Lou, N.; Ungvari, Z.; Goldman, S. A.; Csiszar, A.; et al. Angiogenic Inhibition Reduces Germinal Matrix Hemorrhage. *Nat. Med.* **2007**, *13*, 477–485.

26. Gately, S.; Li, W. W. Multiple Roles of COX-2 in Tumor Angiogenesis: a Target for Antiangiogenic Therapy. *Semin. Oncol.* **2004**, *31*, 2–11.

27. Ueno, T.; Chow, L. W.; Toi, M. Increases in Circulating VEGF Levels During COX-2 inhibitor Treatment in Breast Cancer Patients. *Biomed. Pharmacother.* **2006**, *60*, 277–279.

28. Xu, K.; Gao, H.; Shu, H. K. Celecoxib Can Induce Vascular Endothelial Growth Factor Expression and Tumor Angiogenesis. *Mol. Cancer Ther.* **2011**, *10*, 138–147.

29. Dovizio, M.; Tacconelli, S.; Ricciotti, E.; Bruno, A.; Maier, T. J.; Anzellotti, P.; Di Francesco, L.; Sala, P.; Signoroni, S.; Bertario, L.; et al. Effects of Celecoxib on Prostanoid Biosynthesis and Circulating Angiogenesis Proteins in Familial Adenomatous Polyposis. *J. Pharmacol. Exp. Ther.* **2012**, *341*, 242–250.

30. Jacobson, G. B.; Shinde, R.; Contag, C. H.; Zare, R. N. Sustained Release of Drugs Dispersed in Polymer Nanoparticles. *Angew. Chem., Int. Ed.* **2008**, *47*, 7880–7882.

31. Zhong, Q.; Jin, M.; Xiao, D.; Tian, H.; Zhang, W. Application of Supercritical Anti-Solvent Technologies for the Synthesis of Delivery Systems of Bioactive Food Components. *Food Biophys.* **2008**, *3*, 186–190.

32. Margulis-Goshen, K.; Kesselman, E.; Danino, D.; Magdassi, S. Formation of Celecoxib Nanoparticles from Volatile Microemulsions. *Int. J. Pharm.* **2010**, *393*, 231–238.

33. Margulis-Goshen, K.; Silva, B. F. B.; Marques, E. F.; Magdassi, S. Formation of Solid Organic Nanoparticles from a Volatile Catanionic Microemulsion. *Soft Matter* **2011**, *7*, 9359–9365.

34. Spernath, A.; Aserin, A.; Ziserman, L.; Danino, D.; Garti, N. Phosphatidylcholine Embedded Microemulsions: Physical Properties and Improved Caco-2 Cell Permeability. *J. Controlled Release* **2007**, *119*, 279–290.

35. Zeng, C.-X.; Hu, Q. Determination of the Polyacid Dissociation Constants of Glycyrrhizic Acid. *Indian J. Chem. A* **2008**, *47*, 71–74.

36. Koide, M.; Ukawa, J.; Tagaki, W.; Tamagaki, S. Hydrolysis of Nonionic Ester Surfactants Facilitated by Potassium Beta-glycyrrhizinate: Implication of Catalytic Functions Played by the Carboxyl groups. *J. Am. Oil Chem. Soc.* **1997**, *74*, 49–54.

37. Samanta, D.; Meiser, J. L.; Zare, R. N. Polypyrrole Nanoparticles for Tunable, pH-Sensitive and Sustained Drug Release. *Nanoscale* **2015**, *7*, 9497–9504.

38. Kamoun, E. A.; Chen, X.; Mohy Eldin, M. S.; Kenawy, E.-R. S. Crosslinked Poly(vinyl alcohol) Hydrogels for Wound Dressing Applications: A Review of Remarkably Blended Polymers. *Arabian J. Chem.* **2015**, *8*, 1–14.

39. Hallaway, P. E.; Eaton, J. W.; Panter, S. S.; Hedlund, B. E. Modulation of Deferoxamine Toxicity and Clearance by Covalent Attachment to Biocompatible Polymers. *Proc. Natl. Acad. Sci. U. S. A.* **1989**, *86*, 10108–10112.

40. Allain, P.; Mauras, Y.; Chaleil, D.; Simon, P.; Ang, K. S.; Cam, G.; Le Mignon, L.; Simon, M. Pharmacokinetics and Renal Elimination of Desferrioxamine and Ferrioxamine in Healthy Subjects and Patients with Haemochromatosis. *Br. J. Clin. Pharmacol.* **1987**, *24*, 207–212.

41. Huang, X.; Brazel, C. S. On the Importance and Mechanisms of Burst Release in Matrix-Controlled Drug Delivery Systems. *J. Controlled Release* **2001**, *73*, 121–136.

42. Eberlin, L. S.; Liu, X.; Ferreira, C. R.; Santagata, S.; Agar, N. Y.; Cooks, R. G. Desorption Electrospray Ionization then MALDI Mass Spectrometry Imaging of Lipid and Protein Distributions in Single Tissue Sections. *Anal. Chem.* **2011**, *83*, 8366–8371.

43. Eberlin, L. S.; Tibshirani, R. J.; Zhang, J.; Longacre, T. A.; Berry, G. J.; Bingham, D. B.; Norton, J. A.; Zare, R. N.; Poultsides, G. A. Molecular Assessment of Surgical-Resection Margins of Gastric Cancer by Mass-Spectrometric Imaging. *Proc. Natl. Acad. Sci. U. S. A.* **2014**, *111*, 2436–2441.

44. Eberlin, L. S.; Mulcahy, J. V.; Tzabazis, A.; Zhang, J.; Liu, H.; Logan, M. M.; Roberts, H. J.; Lee, G. K.; Yeomans, D. C.; Du Bois, J.; et al. Visualizing Dermal Permeation of Sodium Channel Modulators by Mass Spectrometric Imaging. *J. Am. Chem. Soc.* **2014**, *136*, 6401–6405.

45. Eberlin, L. S.; Gabay, M.; Fan, A. C.; Gouw, A. M.; Tibshirani, R. J.; Felsher, D. W.; Zare, R. N. Alteration of the Lipid Profile in Lymphomas Induced by MYC Overexpression. *Proc. Natl. Acad. Sci. U. S. A.* **2014**, *111*, 10450–10455.

46. Morosi, L.; Spinelli, P.; Zucchetti, M.; Pretto, F.; Carra, A.; D'Incalci, M.; Giavazzi, R.; Davoli, E. Determination of Paclitaxel Distribution in Solid Tumors by Nano-particle Assisted Laser Desorption Ionization Mass Spectrometry Imaging. *PLoS One* **2013**, *8*, e72532.

47. Margulis-Goshen, K.; Weitman, M.; Major, D. T.; Magdassi, S. Inhibition of Crystallization and Growth of Celecoxib Nanoparticles Formed from Volatile Microemulsions. *J. Pharm. Sci.* **2011**, *100*, 4390–4400.

48. Gupta, P.; Thilagavathi, R.; Chakraborti, A. K.; Bansal, A. K. Role of Molecular Interaction in Stability of Celecoxib-PVP Amorphous Systems. *Mol. Pharmaceutics* **2005**, *2*, 384–391.

49. Inada, T.; Lu, S. S. Inhibition of recrystallization of ice grains by adsorption of poly(vinyl alcohol) onto ice surfaces. *Cryst. Growth Des.* **2003**, *3*, 747–752.

50. Schinkel, A. F. L.; Bax, J. J.; Delgado, V.; Poldermans, D.; Rahimtoola, S. H. Clinical Relevance of Hibernating Myocardium in Ischemic Left Ventricular Dysfunction. *Am. J. Med.* **2010**, *123*, 978–986.

51. Downey, J. M. Heart Failure and Circulatory Shock. In *Essential Medical Physiology*; Johnson, L. R., Ed.; Elsevier: San Diego, CA, 2003; pp 941–949.

52. Solomon, S. D.; McMurray, J. J. V.; Pfeffer, M. A.; Wittes, J.; Fowler, R.; Finn, P.; Anderson, W. F.; Zauber, A.; Hawk, E.; Bertagnolli, M. Cardiovascular Risk Associated with Celecoxib in a Clinical Trial for Colorectal Adenoma Prevention. *N. Engl. J. Med.* **2005**, *352*, 1071–1080.

53. Cochain, C.; Channon, K. M.; Silvestre, J. S. Angiogenesis in the Infarcted Myocardium. *Antioxid. Redox Signaling* **2013**, *18*, 1100–1113.

54. Nakayama, K. H.; Hong, G.; Lee, J. C.; Patel, J.; Edwards, B.; Zaitseva, T. S.; Paukshto, M. V.; Dai, H.; Cooke, J. P.; Woo, Y. J.; et al. Aligned-Braided Nanofibrillar Scaffold with Endothelial Cells Enhances Arteriogenesis. *ACS Nano* **2015**, *9*, 6900–6908.

55. Sant'Anna, R. T.; Kalil, R. A. K.; Moreno, P.; Anflor, L. C. J.; Correa, D. L. C.; Ludwig, R.; Barra, M. B.; Silva, E. A.; Nardi, N.; Sant'Anna, J. R. M.; et al. Gene Therapy with VEGF 165 for Angiogenesis in Experimental Acute Myocardial Infarction. *Rev. Bras. Cir. Cardiovasc.* **2003**, *18*, 142–147.

56. Shakeel, F.; Baboota, S.; Ahuja, A.; Ali, J.; Shafiq, S. Skin Permeation Mechanism and Bioavailability Enhancement of Celecoxib from Transdermally Applied Nanoemulsion. *J. Nanobiotechnol.* **2008**, *6*, 8–11.

57. Dvir, T.; Bauer, M.; Schroeder, A.; Tsui, J. H.; Anderson, D. G.; Langer, R.; Liao, R.; Kohane, D. S. Nanoparticles Targeting the Infarcted Heart. *Nano Lett.* **2011**, *11*, 4411–4414.

58. Kolk, M. V.; Meyberg, D.; Deuse, T.; Tang-Quan, K. R.; Robbins, R. C.; Reichenspurner, H.; Schrepfer, S.

LAD-Ligation: a Murine Model of Myocardial Infarction. *J. Visualized Exp.* **2009**, 10.3791/1438.

59. Swijnenburg, R. J.; Govaert, J. A.; van der Bogt, K. E.; Pearl, J. I.; Huang, M.; Stein, W.; Hoyt, G.; Vogel, H.; Contag, C. H.; Robbins, R. C.; et al. Timing of Bone Marrow Cell Delivery Has Minimal Effects on Cell Viability and Cardiac Recovery After Myocardial Infarction. *Circ. Cardiovasc. Imaging* **2010**, *3*, 77–85.